ACS APPLIED MATERIALS & INTERFACES

Research Article

Cite This: ACS Appl. Mater. Interfaces 2019, 11, 32192−32199

www.acsami.org

Manipulating Localized Vibrations of Interstitial Te for Ultra-High Thermoelectric Efficiency in p-Type Cu−In−Te Systems

Ting Ren,[†,‡] Zhongkang Han,[*,§] Pengzhan Ying,[‡] Xie Li,[†] Xiaoyan Li,[§] Xinyi Lin,[$] Debalaya Sarker,[*,#] and Jiaolin Cui[*,†]

[†]School of Materials and Chemical Engineering, Ningbo University of Technology, Ningbo 315211, China

[‡]School of Materials Science and Engineering, China University of Mining and Technology, Xuzhou 221116, China

[§]Division of Interfacial Water and Key laboratory of Interfacial Physics and Technology, Shanghai Institute of Applied Physics, Chinese Academy of Sciences, Shanghai, 201800, China

[$]Department of Mechanical Engineering and Materials Science, Duke University, Durham, North Carolina 27708, United States

[#]Theory Department, Fritz-Haber Institute of the Max Planck Society, Faradayweg 4-6, Berlin 14195, Germany

Supporting Information

ABSTRACT: Thermoelectric materials are of imperative need on account of the worldwide energy crisis. However, their efficiency is limited by the interplay of high electrical and lower thermal conductivities, that is, the figure of merit (ZT). Owing to their unique crystal structures, Cu−In−Te-based chalcogenides are suitable for both and thus have attracted much attention recently as potential thermoelectrics. Here we explore a newly developed Cu−In−Te derivative compound $Cu_{3.52}In_{4.16}Te_8$. With a proper adjustment of Cu_2Te doping, this material shows an ultralow lattice thermal conductivity (κ_L) (0.3 $WK^{-1}m^{-1}$) and, consequently, a figure of merit (ZT) as high as 1.65(±0.15) at 815 K: the highest value reported for p-type Cu−In−Te to date. The reduction in κ_L is directly related to the alteration of local symmetry around the interstitial Te, resulting in an effectively optimized phonon transport through localized "rattling" of the same. Although the Hall carrier concentration reduces upon Cu_2Te addition due to the unpinning of the Fermi level (E_{Fermi}) toward the conduction band minimum, the power factor remains stable. The knowledge depicted here not only demonstrates the potential of $Cu_{3.52}In_{4.16}Te_8$-based alloys as a promising TE, but also provides guidelines for developing further high-performance thermoelectric materials by enhancing the electronic conductivity.

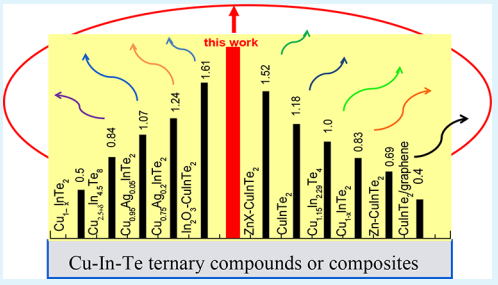

KEYWORDS: *thermoelectric performance, $Cu_{3.52}In_{4.16}Te_8$, ultralow lattice thermal conductivity, phonon spectrum, band structure*

INTRODUCTION

The conversion of thermal energy to electricity by thermoelectric (TE) devices is believed to play a key role in solving the future energy crisis. The efficiency of TE performance is largely determined by the dimensionless figure of merit (ZT), which is characterized by the equation: $ZT = T\alpha^2\sigma/\kappa$, where T, α, σ, κ are, respectively, the absolute temperature, Seebeck coefficient, electrical conductivity, and total thermal conductivity consisting of mainly lattice (κ_L) and electronic (κ_e) parts. To maximize the ZT value, a high power factor ($\alpha^2\sigma$) and low κ are essential requirements. Since the three parameters α, σ, and κ_e are interrelated; it is very difficult to decouple them. κ_L being the only independently tunable parameter, many approaches viz. all-scale hierarchical nano-mesostructuring,[1,2] magnetoelectric or thermoelectromagnetic interactions in the bulk matrix,[3] explorations of liquid-like compounds,[4,5] and entropy driven enhanced point defects in solid solution GeSe[6] etc., have been extensively applied to reduce it. Moreover, κ_L is closely related to the disturbances of the lattice structure or unusual vibrational properties. For example, the electrostatic repulsion between the lone s^2 pair at Sb sites in Cu(Ag)−Sb-Se compounds yields soft frequency modes and high Grüneisen parameters, thus reducing the κ_L to as low as 0.25 $Wm^{-1}K^{-1}$.[7−9] In binary selenides, anisotropic bonding in SnSe,[10] bonding asymmetry in InTe[11] and soft localized vibrations of bismuth bilayer in BiSe[12] are responsible for their ultralow κ_L. The newly observed appearances, such as hierarchical or multicenter chemical bonds in α-MgAgSb,[13] CdSb,[14] $AgBi_3S_5$,[15] and low sound velocity or cutoff frequency of acoustic phonons in Ag_8SnSe_6,[16] Ag_9GaSe_6,[17] $AgInSe_2$,[18] AgCuTe,[19] and $Bi_{13}S_{18}I_2$[20] make the phonon scattering intensified enough for a low κ_L value and, hence, high TE performance. Now, Te, being heavier than Se or S, not only possesses a lower κ_L, but also tends to form weaker bonds because of its lower electronegativity. Indeed, AgCuTe,[19] $CsBi_4Te_6$,[21] and Zn doped GeSbTe[22] etc. are reportedly few of the many state-of-the-art TE telluride materials.

Received: July 12, 2019
Accepted: August 14, 2019
Published: August 23, 2019

The advantage of tunable band-structure in Te based TE materials, however, has not yet been fully explored. Mainly, the research lacks the investigations relating to the increased phonon scattering, caused by inducing the dynamic disorder due to interstitially residing anions in the lattice.

Owing to the inherent presence of cation vacancy and unique crystal structures, Cu−In−Te ternary compounds with a chalcopyrite structure (e.g. $I\bar{4}2d$) have recently attracted much attention in thermoelectrics.[23−26] Examples include experimentally prepared $Cu_{0.95}Ag_{0.05}InTe_2$ (ZT = 1.07 at 823 K),[27] $Cu_{0.75}Ag_{0.2}InTe_2$ (ZT = 1.24 at ∼850 K),[28] In_2O_3−$CuInTe_2$[29] and ZnX-$CuInTe_2$.[30] Since the cation vacancy engineering in these compounds can be used to tune the density of carrier (n) (or mobility μ),[31,32] similar to those observed in many Cu−Ga−Te compounds,[33−36] the TE performance can get vastly improved. However, the versatility of these Cu−In−Te chalcogenides as TE candidates has not been explored to the fullest until now. Nevertheless, the endless possibilities of tuning the structural parameters, viz. doping or vacancy concentrations, allows one to optimize the electronic and vibrational properties of Cu−In−Te-based chalcopyrite compounds to further achieve better TE performance.

Inspired by the above-mentioned pioneering works, we aim to tune the lattice anharmonicity and additional phonon modes in an another newly developed ternary Cu−In−Te chalcogenide $Cu_{3.52}In_{4.16}Te_8$ compound, in addition to $Cu_{1.15}In_{2.29}Te_4$[37] and $Cu_{2.5+\delta}In_{4.5}Te_8$.[38] Besides, this compound with inherent Cu-poor and In-rich comparing with the pristine $CuInTe_2$ may have more room to regulate the band structures by adjusting the doping concentration of Cu_2Te. For an intermediate doping amount (x = 0.08), we observe an ultralow lattice thermal conductivity and a subsequent high ZT value of 1.65 ± ∼ 0.15 at 815 K. By a combined experimental and density functional approach based theoretical understanding, we demonstrate that local structural disorder caused by an interstitial Te atom provides additional "rattling" modes for phonon scattering, which leads to the high n or μ and low κ_L features in the material.

EXPERIMENTAL SECTION

Syntheses and Preparation of Samples. To achieve the desired doping concentrations in $(Cu_2Te)_x(Cu_{3.52}In_{4.16}Te_8)$ (x = 0, 0.03, 0.05, 0.08, 0.11), the mixtures of three elements (Cu, In, and Te with the purity of more than 99.999%, Emei Semicon. Mater. Co., Ltd. Sichuan, CN), are loaded into five different silica vacuum tubes for melting. The melting is conducted at 1123 K for 24 h, followed by 800 K annealing for 72 h. During the melting process, the samples are rocked for 30 s every 1 h to minimize segregation. After cooling down to room temperature (RT), the ingots are ball milled at a rotation rate of 350 rpm for 5 h in stainless steel bowls that contain benzinum. The dried powders are then rapidly sintered using spark plasma sintering apparatus (SPS-1030) at a peak temperature of ∼900 K and a pressure of 50 MPa. The densities (d) of the polished bulks, ranging from 6.0−6.2 × 10^{-3} kg/cm^3, are measured using Archimedes' method.

The bulk samples with sizes of about 2.5 × 3 × 12 mm^3 and 2 × 2 × 7 mm^3 are prepared for electrical property and Hall coefficient measurements respectively, and those of ϕ10 × 1.5 mm^2 for thermal diffusivity measurement.

Analyses and Measurements. Powder X-ray diffractions for all synthesized samples are recorded on a powder X-ray diffractometer (D8 Advance) operating at 40 kV and 40 mA at Cu Kα radiation (λ = 0.15406 nm) in the range from 10° to 110° with a step size of 0.02°. Besides, X'Pert Pro, PANalytical code is used to do the Rietveld refinement of the XRD patterns of the pristine $Cu_{3.52}In_{4.16}Te_8$ and Cu_2Te-alloyed samples. This refinement is conducted with a step size of 0.01°, ranging from 10° to 100° using the same operating voltage and current, as shown in Supporting Information (SI) Table S2.

Hall coefficients (R_H) are measured by using a four-probe configuration in PPMS (Model-9) with a magnetic field up to ±2 T. The Hall mobility (μ) and carrier concentration (n_H) are calculated according to the relations $\mu = |R_H|\sigma$ and $n_H = 1/(e\ R_H)$ respectively, where e is the electron charge.

Electrical conductivity and Seebeck coefficients are measured simultaneously under a helium atmosphere from RT to ∼815 K in a ULVAC-RIKO ZEM-3 instrument system with an uncertainty of <6.0% each. The thermal diffusivities (λ) are measured by TC-1200RH instrument in a vacuum with an uncertainty of <10.0%. The Dulong−Petit rule is used to estimate the heat capacities (C_p) above RT. The thermal conductivities are then calculated based on the equation $\kappa = d\lambda C_p$. The three physical parameters (α, σ, κ) are finalized by taking the average values of several samples tested by the same method. The lattice contribution (κ_L) is the total κ minus the electronic contribution (κ_e). Here, κ_e is expressed by the Wiedemann−Franz (W−F) relation, $\kappa_e = L_0\sigma T$, where L_0 is the Lorenz number, estimated using the formula L_0 = 1.5+exp(−|α|/116)[39] (where L_0 is in 10^{-8} WΩK^{-2} and |α| in μVK^{-1}). The TE figure of merits (ZTs) are then calculated using the three parameters mentioned above with the total uncertainty of about 18%.

Differential scanning calorimeter (DSC) is conducted in a Netzch STA 449 F3 Jupiter equipped with a TASC414/4 controller. The instrument is calibrated from a standard list. The sample of the powder (x = 0.08) is loaded into an open alumina crucible. The measurement is performed between ∼305 K to ∼827 K with a heating rate of 5 K min^{-1} in Ar atmosphere.

Methodology. First-principles calculations are carried out with FHI-aims,[40,41] an all-electron, full-potential electronic-structure code under the framework of density-functional theory (DFT).[42] FHI-aims uses numeric atom-centered basis sets, where numerical settings are so chosen for the present study that a convergence in energy differences better than 10^{-3} eV/atom is achieved. Both the atomic coordinates and lattice vectors are fully relaxed for all structures Generalized gradient approximation is used for electronic exchange and correlation as per Perdew Burke Enzerhof (PBE).[43] We have calculated the electronic structure with more advanced Heyd-Scuseria-Ernzerhof hybrid functional (HSE06),[44] which takes into account the fraction of exact exchange.

For phonon dispersion calculations, we have used the finite displacement method within the harmonic approximations, as is implemented in the Phonopy code.[45] The mode-resolved phonon group velocity v_g^i (=dω_i/dk), and Grüneisen parameters γ_i (=1/ω_idω_i/dV) are extracted from the phonon dispersions. For calculating g, the lattice is strained by 2%. The chosen numerical settings are indicated in the Supporting Information.

RESULTS AND DISCUSSION

SEM and XRD Analyses. A SEM image of a freshly fractured surface for the sample with x = 0 is shown in SI Figure S1. The sample is dense with no observable pores or cracks. The EDS mappings of the selected area (highlighted by the yellow box in SI Figure S1a) demonstrate that all three elements Cu, In, and Te (SI Figure S1b−d) are slightly segregated. The average chemical compositions of Cu, In, and Te in $(Cu_2Te)_x(Cu_{3.52}In_{4.16}Te_8)$ (x = 0, 0.08) are roughly the same as those of the nominal ones, see SI Table S1, where the numbers of Te moles are normalized to 8.0 (x = 0) and 8.08 (x = 0.08). These results indicate that the materials have been synthesized as intended.

The refinements of the powder X-ray diffraction (XRD) patterns of $(Cu_2Te)_x(Cu_{3.52}In_{4.16}Te_8)$ (x = 0, 0.05, 0.08, 0.11) are shown in SI Figure S2. The results involving the Wyckoff positions, atomic coordinates, and site occupancy factors

DOI: 10.1021/acsami.9b12256
ACS Appl. Mater. Interfaces 2019, 11, 32192−32199

(SOFs) are listed in SI Tables S2–S6, where the SOFs of Cu (4a), In (4b), and Te (8d) are all 1.0. It can be seen that the main peaks of the patterns are indexed to the existing chalcopyrite $CuInTe_2$ (PDF: 65–0245) with no impurities precipitated. Figure 1 and SI Table S2 present the lattice

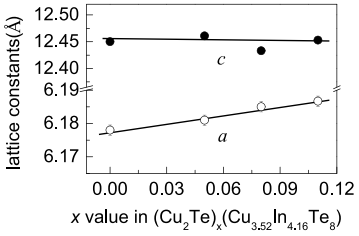

Figure 1. Relationship between the lattice constants and Cu_2Te content. It is observed that the lattice parameter a increases almost linearly, and follows the Vegard's law.

constants as a function of Cu_2Te content, where we observe that lattice constant (a) tends to increases, whereas the c value tends to decrease as x value increases. This is indicative of the expansion tendency of the crystal. However, the tetragonal distortion parameter η value ($\eta = c/2a$) reduces from 1.008 to 1.005, suggesting that the crystal structure distortion tends to weaken.

In order to gain a deep understanding of thermal stability of the materials, the DSC analysis of the material (x = 0.08) reveals an exothermic effect at 333.7 °C (~607 K) corresponding to a phase transition (SI Figure S3a). Besides, from the high temperature XRD patterns (623 K-823 K) (SI Figure S3b), we attain the same value of the lattice constants ($a = b = c$ = 6.1654–6.2005 Å) for each temperature (see SI Table S7), even though the main diffraction peaks in SI Figure S3b do not change. The above analyses confirm that the ordered chalcopyrite structure has already been transformed into the disordered sphalerite structure (η = 1) above 623 K, since the disordered phase is indeed stable at high temperatures. The driving force for the order–disorder phase transition is likely due to the Cu–In antisite occupancy starting in the critical temperature range.[46−48] After the transition, the crystal structure distortion diminishes, which thereby weakens the phonon scattering from the crystal structure point of view. However, the local disorder created by the point defects, such as copper vacancy and interstitial Te, still remains.

Lattice Thermal Conductivities and Phonon Spectra. Figure 2a presents the lattice thermal conductivities (κ_L) as a function of temperature, where the lattice parts overall show a mixed trend. At temperatures lower than ~650 K, the lattice parts enhance with increasing Cu_2Te content, as shown in Figure 2a inset. However, at higher temperatures than ~650 K, the κ_L value generally reduces as Cu_2Te content increases. It is notable that the sample at x = 0.08 gives an ultralow κ_L value (0.30 $WK^{-1}m^{-1}$) at 815 K, which is about a 40% drop in comparison to that at x = 0. However, the κ_L values at x = 0.11 are a little higher than those at x = 0.08.

Such a mixed trend has also been observed in MnTe-SnTe,[49] $Mg_2(Si, Sn)$[50] systems and is usually related to the complex phonon scattering mechanisms.

In this work, we did not detect any impurity phases at high temperatures from the high temperature XRD, nor did we observe them using the high resolution TEM (HRTEM), see

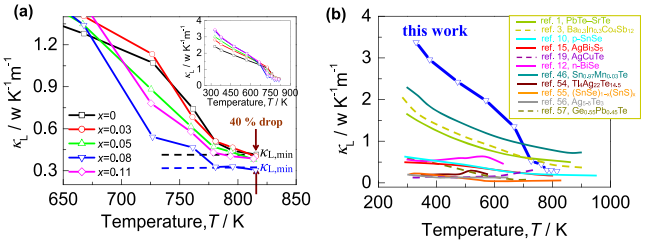

Figure 2. (a) Experimentally determined lattice thermal conductivities (κ_L) of $(Cu_2Te)_x(Cu_{3.52}In_{4.16}Te_8)$ (x = 0, 0.03, 0.05, 0.08, 0.11) as a function of temperature. The estimated minimum $\kappa_{L,min}$ for $Cu_{27}In_{33}Te_{64}$ and $Cu_{29}In_{33}Te_{65}$ is 0.42 and 0.33 $WK^{-1}m^{-1}$, respectively, symbolized by dashed lines. (b) Comparison of the κ_L values in this work with others.

SI Figure S4. The measured density of the materials ranges from 6.0 × 10^{-3} kg/cm^{-3} to 6.2 × 10^{-3} kg/cm^{-3}, which is comparable to the theoretical density (6.087 × 10^{-3} kg/cm^{-3}) of $CuInTe_2$. Therefore, the effects of the morphology, density and microstructures etc. on phonon scattering can be ruled out in different materials. Therefore, it is the interplay of Cu vacancy (V_{Cu}) and interstitial Te at different concentrations that leads to the above anomalous behavior in the present work. The V_{Cu} concentration is reduced as Cu_2Te content increases, which weakens the phonon scattering at Cu vacancies. However, at high temperatures, the local strain created by the interstitial Te seems to play a dominant role in affecting the phonon transport, as is also observed in Sb-$CuCr_2S_4$,[51] $Cu_2ZnGeSe_{4-x}Sx$,[52] and $CsAg_5Te_3$[53] systems. Besides, the dominant effect of interstitial Te unravels the rapid reduction in κ_L at high temperatures as Cu_2Te content increases. An enhancement in κ_L at x = 0.11 originates from a dual effect: saturation of the interstitial Te in the lattice and reduction in Cu vacancy with increased Cu_2Te content.

The measured low lattice thermal conductivities (0.43 $WK^{-1}m^{-1}$ for x = 0 and 0.30 $WK^{-1}m^{-1}$ for x = 0.08) at 815 K are a little higher than those of the state-of-the-art TE materials, such as $AgBi_3S_5$ (0.25 $WK^{-1}m^{-1}$),[15] AgCuTe (0.2 $WK^{-1}m^{-1}$),[19] n-BiSe,[12] $CsAg_5Te_3$ (0.18 $WK^{-1}m^{-1}$),[53] $Tl_2Ag_{12}Te_{7+\delta}$ (0.25 $WK^{-1}m^{-1}$),[54] SnSe (0.11–0.23 $WK^{-1}m^{-1}$),[10,55] $Ag_{5-\delta}Te_3$ (0.2 $WK^{-1}m^{-1}$),[56] and $Ge_{0.55}Pb_{0.45}Te$ (0.23 $WK^{-1}m^{-1}$),[57] but lower than those of PbTe–SrTe (0.5 $WK^{-1}m^{-1}$),[1] $Ba_{0.3}In_{0.3}Co_4Sb_{12}$ (0.6 $WK^{-1}m^{-1}$),[3] and $Sn_{0.97}Mn_{0.03}Te$ (0.5 $WK^{-1}m^{-1}$),[49] see Figure 2b.

On the other hand, these measured κ_L values at 815 K are comparable to or even a little lower than the estimated $\kappa_{L,min}$ values (0.42 $Wm^{-1}K^{-1}$ for x = 0 and 0.33 $Wm^{-1}K^{-1}$ for x = 0.08, respectively), see horizontal dashed lines in Figure 2a, based on the glass limit model of Cahill et al.,[58]

$$\kappa_m = \frac{1}{2}\left(\frac{\pi}{6}\right)^{1/3} \kappa_B V^{-2/3}(2\nu_T + \nu_L) \quad (1)$$

here the ν_T and ν_L values are the average velocities displayed in Table 1, which are directly calculated using the phonon spectra discussed below.

The unexpectedly low lattice part κ_L can be observed in many systems, such as Cu–Sb–Se[9] and $Ge_{1-x}Mn_xTe$,[59] due to the fact that the Cahill model does not take into account the effect of a periodic boundary condition on the phonon dispersion, thus overestimating the group velocity for high-frequency phonons.[60] Chen et al. reported that in some

DOI: 10.1021/acsami.9b12256
ACS Appl. Mater. Interfaces 2019, 11, 32192–32199

Table 1. Phonon Velocities in the Vicinity of Brillouin Zone Center (v_{LA}, v_{TA1}, v_{TA2}) for Longitudinal (LA) and Transverse (TA1, TA2) Acoustic Phonon Branches Along the Γ−*X*, Γ−*W*, and Γ−*L* Directions Based on the Phonon Spectra[a]

$Cu_{27}In_{33}Te_{64}$ (v in m/s)				$Cu_{29}In_{33}Te_{65}$ (v in m/s)			
directions	v_{TA1} (m/s)	v_{TA2} (m/s)	v_{LA} (m/s)	directions	v_{TA1} (m/s)	v_{TA2} (m/s)	v_{LA} (m/s)
Γ-*x*	1232	1425	2294	Γ−*x*	1165	1374	2424
Γ-*w*	1777	1777	3633	Γ−*w*	1885	2042	3532
Γ-*L*	2341	2951	5852	Γ−*L*	1464	1673	2898
average ν_m	1783	2051	3926	average ν_m	1504	1696	2951

[a]The average phonon velocities are taken as the average values of the three directions.

material systems the $\kappa_{L,min}$ values could be ∼40% lower than those estimated by Debye-Cahill model.[60]

Although the XRD refinements reveal that the elements Cu and Te totally reside at the 4a and 8d sites, respectively, the first-principles calculation indicates that Cu is energetically favorable to the Cu vacancy site, rather than the interstitial site, as the energy is ∼0.3 eV higher than that at the Cu vacancy if Cu resides at the interstitial site. In addition, we also calculate the possibility of Te residing at the Cu vacancy, but find it is not possible either because such an occupation is not stable and Te is inclined to diffuse to its neighbor interstitial site during the geometry relaxation processes. Therefore, the atomic occupations in the present material system are different from those in Cu_2Se-doped PbSe[61] and Cu_2Te-doped PbTe systems,[62] in which the element Cu interstitially resides at the lattice structures.

Based on the above analyses relating to the atomic occupations, we present a comparative analysis of phonon spectra of $Cu_{3.52}In_{4.16}Te_8$ with and without interstitial Te in the crystal structure, determined from first-principles calculations to unravel the underlying reason for low κ_L. Figure 3a and b are

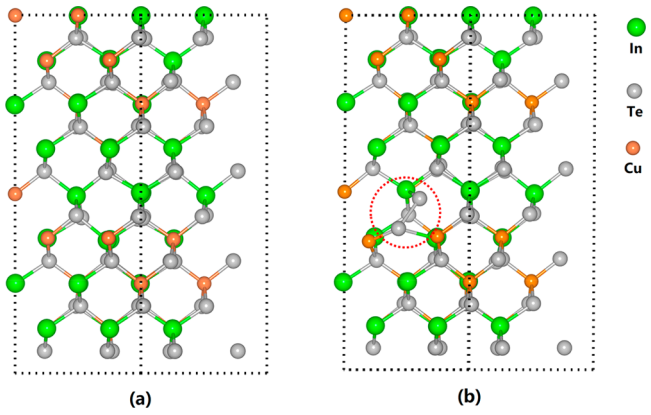

Figure 3. Crystal structures of (a) $Cu_{27}In_{33}Te_{64}$ (corresponding to $Cu_{3.52}In_{4.16}Te_8$); (b) $Cu_{29}In_{33}Te_{65}$ (corresponding to $(Cu_2Te)_{0.11}(Cu_{3.52}In_{4.16}Te_8)$ with interstitial Te in the lattice.

the crystal structures of $Cu_{27}In_{33}Te_{64}$ (corresponding to $Cu_{3.52}In_{4.16}Te_8$) without interstitial Te and $Cu_{29}In_{33}Te_{65}$ (corresponding to $(Cu_2Te)_{0.11}(Cu_{3.52}In_{4.16}Te_8)$ with interstitial Te, respectively. It is observed that the In−Te bond length changes around the interstitial Te, which is highlighted in a red dotted circle (Figure 3b).

The phonon spectra corresponding the above crystal structures are presented in Figure 4a and b. Upon doping of Cu_2Te, that is, interstitial occupation of Te, the neighboring framework Te atoms shift from their crystallographic sites, thus providing"rattling" sites for phonon scattering. The rattling

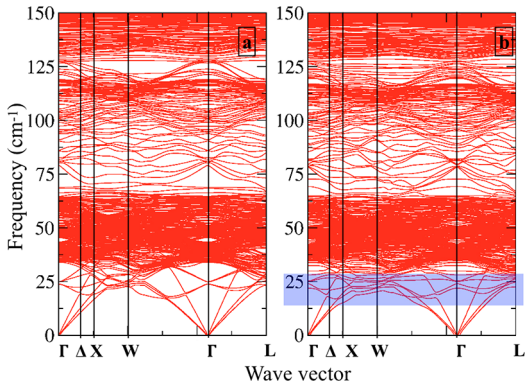

Figure 4. Phonon spectra. (a) without Cu_2Te-doped system ($Cu_{27}In_{33}Te_{64}$), (b) with Cu_2Te-doped system ($Cu_{29}In_{33}Te_{65}$). Upon doping of Cu_2Te, that is, occupation of interstitial Te, the neighboring framework Te atoms shift from their crystallographic sites, thus providing "rattling" sites for phonon scattering. The rattling modes near the low frequency acoustic branches (around 25 cm^{-1}) can be clearly seen.

modes near the low frequency acoustic branches (around 25 cm^{-1}) in Figure 4b can be clearly seen. This localized mode of Te defects hybridize with the low frequency acoustic modes and plays a crucial role in scattering phonons, leading to a significant reduction of the lattice thermal conductivity. Besides, a tiny overall down-shift of the modes are observed in the Cu_2Te doped system as compared to the undoped one. This is due to the increase in In−Te bond distance after doping, thus weakening the bond strength and subsequently further reducing the lattice thermal conductivity of the system. The calculations in this work is in agreement with our experimental findings.

Moreover, the zone center group velocities of acoustic phonon branches are calculated for the Γ−X, Γ−W, and Γ−L directions, respectively, and the average sound velocities (average for the three directions) are estimated according to the phonon spectra, as shown in Table 1. The average sound velocity for each branch of $Cu_{27}In_{33}Te_{64}$ (v_{TA1} = 1783 (m/s), v_{TA2} = 2051 (m/s), v_{LA} = 3926 (m/s)) is much higher than that of $Cu_{29}In_{33}Te_{65}$ (v_{TA1} = 1504 (m/s), v_{TA2} = 1696 (m/s), v_{LA} = 2951 (m/s)). The Debye Temperatures of $Cu_{27}In_{33}Te_{64}$ for three branches, calculated on the basis of the above sound velocities, are a little higher than those of $Cu_{29}In_{33}Te_{65}$ either, see Table 2. Besides, the average Debye temperatures (201° and 165°) in these two compounds are comparable to that of α-MgAgSb (201 K),[13] CuAgTe (179 K),[19] BiSe (195 K),[12] and $CuInTe_2$ (197.5 K),[63] but are lower than that of $CuGaTe_2$ (229 K).[64] The Grüneisen parameters are shown in Figure 5. The average values of 3.069, 1.956, and 1.258 for γ_{TA1}, γ_{TA2}, and γ_{LA}, respectively are indicative of the high anharmonicity of the doped compound. The reduced sound velocity and

DOI: 10.1021/acsami.9b12256
ACS Appl. Mater. Interfaces 2019, 11, 32192−32199

Table 2. Debye Temperatures (Θ_{LA}, Θ_{TA1}, Θ_{TA2}) for Longitudinal (LA) and Transverse (TA1, TA2) Acoustic Phonon Branches[a]

system	Θ_{TA1}(K)	Θ_{TA2}(K)	Θ_{LA}(K)	$\Theta_{ave.}$(K)
$Cu_{27}In_{33}Te_{64}$	136	196	272	201
$Cu_{29}In_{33}Te_{65}$	131	204	162	165

[a]The mode Debye temperatures are calculated using $\Theta = \hbar\omega_m/2\pi k_B$, where $\omega_m = \left[v_m 6\pi^2\left(\frac{N}{V}\right)\right]^{1/3}$, and k_B is the Boltzmann constant, V is the volume per atom, N atomic numbers in a unit cell.

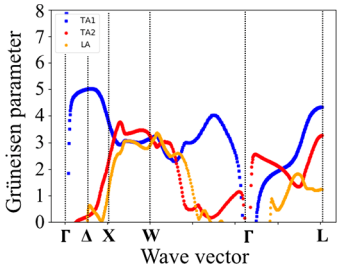

Figure 5. Mode Grüneisen dispersions for $Cu_{29}In_{33}Te_{65}$. The average values of 3.069, 1.956, and 1.258 for γ_{TA1}, γ_{TA2}, and γ_{LA}, respectively, are indicative of the high anharmonicity of the doped compound.

Debye Temperature along with high Grüneisen parameters upon Cu_2Te addition reflect overall weakening of chemical bonds, thus further elucidating the reason behind experimentally determined reduction of lattice part of κ_L.

Band Structures and Electrical Properties. Upon residing of interstitial Te, the electronic structure gets modified. It is evident from the total density of states (DOS) of Figure 6a and b that the additional Cu_2Te causes a shift in

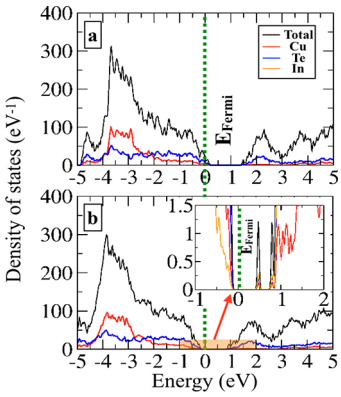

Figure 6. Electronic density of states of (a) undoped and (b) doped system. Inset in (b) shows the zoomed view near the Fermi level (E_{Fermi}).

Fermi level (E_{Fermi}) (defined as $E_{Fermi} = 0$) toward the conduction band minimum (CBM). Alternatively, for the convenience of understanding, we could also replot the DOS without shifting the Fermi level(s), as shown in SI Figure S5, where the Fermi energy (E_{Fermi}) is at ~ −5.5 eV for the undoped system (top panel) and is at ~ −5.1 eV for the doped one (bottom panel). Based on this calculation, it can be seen that the Fermi energy still shifts toward the CBM after doping. It is noted that after doping, the new states create within the gap (see zoomed view of the "near-Fermi" region). These new states not only originate from the interstitial Te atoms, but also are hybridized with states of In, Te, and Cu. This modifies the local crystal structure and changes the electronic structure of the system. The movement of E_{Fermi} toward CBm would suppress the number of p-type carriers. The creation of new states, however, has a dual effect: acting as an e−h recombination center[65] and/or reducing the band gap that promotes the transport of carriers.[66]

In order to further elucidate the origin of the variation in transport properties upon doping, the Hall coefficients at room temperature (RT) are measured. The carrier density (n_H) and mobility (μ) are extracted and shown in Figure 7. The Hall

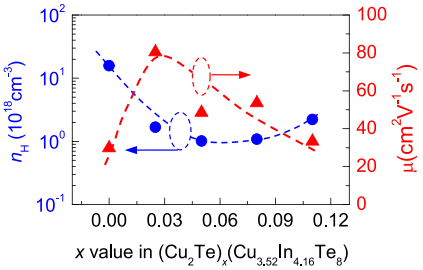

Figure 7. (a) Hall carrier densities (n_H) and mobility (μ) of the $(Cu_2Te)_x(Cu_{3.52}In_{4.16}Te_8)$ measured at RT.

carrier concentration decreases from 1.56×10^{19} cm^{-3} at $x = 0$ to 1.01×10^{18} cm^{-3} at $x = 0.05$, and then increases slightly, while the mobility increases from 29.7 cm^{2}V^{-1}s^{-1} ($x = 0$) to 80.4 cm^{2}V^{-1}s^{-1} ($x = 0.03$), and then decreases. It is, therefore, concluded that the dominant reduction in n_H is due to the movement of E_{Fermi} toward the CBM, while the slight enhancement in n_H at $x > 0.05$ might be caused by the reduction of the band gap, which promotes the acceptor-type carriers from the valence band to the new states.[66]

The temperature-dependent Seebeck coefficients (α) and electrical conductivities (σ) of $(Cu_2Te)_x(Cu_{3.52}In_{4.16}Te_8)$ compounds are shown in Figure 8a,b, respectively. The positive α values are indicative of p-type semiconducting behavior. It is noted that the α value at low temperatures increases with increasing x value until $x = 0.05$ is reached. However, the σ value at high temperatures gradually increases with x value increasing in all the composition range. The variation of the σ value with composition is opposite to that of

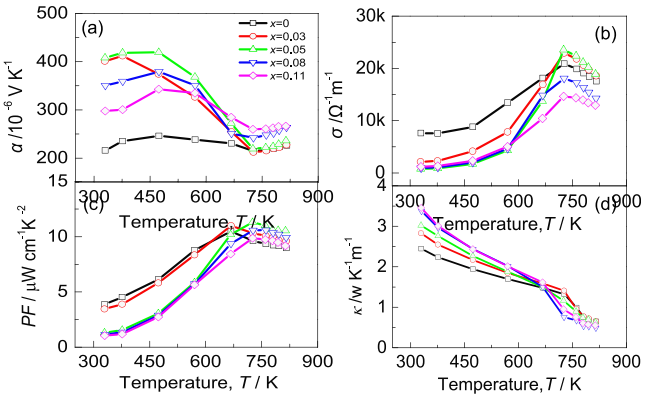

Figure 8. TE performance of $(Cu_2Te)_x(Cu_{3.52}In_{4.16}Te_8)$ with different Cu_2Te contents. (a) Seebeck coefficients (α) as a function of temperature; (b) Electrical conductivities (σ) as a function of temperature; (c) Power factors (PF) as a function of temperature; and (d) Total thermal conductivities (κ) as a function of temperature.

DOI: 10.1021/acsami.9b12256
ACS Appl. Mater. Interfaces 2019, 11, 32192−32199

the Seebeck coefficient. The highest σ value at $x = 0.08$ reaches $1.81 \times 10^4\ \Omega^{-1}m^{-1}$ at 727 K (see Figure 8b), which gives the highest power factor PF = 10.60 $\mu Wcm^{-1}K^{-2}$ (Figure 8c). Besides, the temperature and composition dependence of total thermal conductivity (κ) bear resemblance to those of the lattice part κ_L (Figure 2a), indicating that the phonon transport plays a dominant role in heat carrying. The lowest κ for the sample at $x = 0.08$ is 0.49 $WK^{-1}m^{-1}$ at 815 K, see Figure 8d.

Combined with the above three parameters (α, σ, and κ), we attained the ZT values as a function of temperature, which are calculated and shown in Figure 9a. We note that the sample at

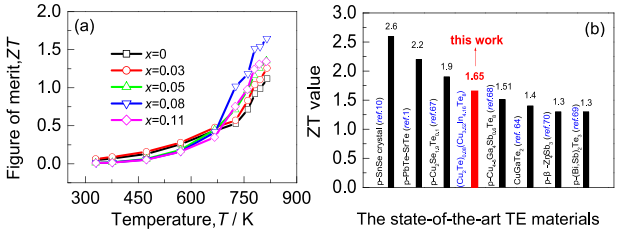

Figure 9. (a) TE figure of merit (ZT) as a function of temperature for different Cu_2Te contents in $(Cu_2Te)_x(Cu_{3.52}In_{4.16}Te_8)$, among which the highest ZT value of 1.65 ± 0.15 was attained at $x = 0.08$ and 815 K; (b) Comparison of the ZT value in this work with those of the state-of-the-art TE materials.

$x = 0.08$ gives the highest ZT value of 1.65 (±0.15) at 815 K, which is a 1.5 fold enhancement as compared with $x = 0$ compound. Although the highest ZT value is lower than those of state-of-the-art TE materials, such as, p-PbTe (ZT = 2.2),[1] SnSe (ZT = 2.6),[10] and p-$Cu_2Se_{1.9}Te_{0.1}$ (ZT = 1.9),[67] but comparable to or higher than those of p-$Cu_{4-\delta}Ga_4Sb_{0.6}Te_8$ (ZT = 1.51),[68] p-$CuGaTe_2$ (ZT = 1.4),[64] p-$(Bi,Sb)_2Te_3$ (ZT = 1.3),[69] and p-β-Zn_4Sb_3 (ZT = 1.3),[70] as shown in Figure 9b. This indicates that the studied material has great potential for industry.

In order to check the thermal stability of the samples, the measurements of the TE performance in cooling cycle have been conducted at $x = 0.08$, and the results are shown in SI Figure S6a–d. It is observed that the electrical conductivities (σ) and thermal conductivities (κ) are a little higher than those in the heating process, whereas the Seebeck coefficients (α) are a little lower over the entire temperature range. The resultant ZT values are ∼12% lower than those in the heating process, probably due to the evaporation of the element Te according to the TG signal in $Cu_{2.5}In_{4.5}Te_8$ reported in ref 28. However, this error is still within the measurement uncertainty.

Nevertheless, we find that the improved TE performance in this work does not rely much on the enhancement in power factor (PF), since the highest PF value at $x = 0.08$ is comparable to that at $x = 0$ (10.48 $\mu Wcm^{-1}K^{-2}$) (see Figure 8c). Therefore, we can conclude that the improvement in TE performance is largely driven by the reduction in lattice thermal conductivity. As such, it can be understood that the localized "rattling" of interstitial Te through Cu_2Te doping effectively optimizes the phonon transport in p-type $Cu_{3.52}In_{4.16}Te_8$ system, and responsible for the remarkable improvement in TE performance.

In this work it should be pointed out that the Hall carrier concentration (1.1×10^{18} cm^{-3}) at which the ZT value gets the highest does not reach the optimal one ($10^{19} \sim 10^{20}$ cm^{-3}),[71] which implies that the TE performance of current materials $(Cu_2Te)_x(Cu_{3.52}In_{4.16}Te_8)$ still has room to be improved if one synergistically optimizes the electronic properties.

CONCLUSIONS

A new p-type Cu−In−Te derivative $Cu_{3.52}In_{4.16}Te_8$ is synthesized and studied in detail with different Cu_2Te doping. The highest ZT value of 1.65 (±0.15) has been attained for the sample with a proper Cu_2Te ($x = 0.08$) doping at 815 K, which makes the performance of this material stand tall in the current state-of-the-art TE community. The origin of the high TE performance is demonstrated to be mainly due to the significant reduction in lattice contribution κ_L, caused by the localized "rattling" of interstitial Te that weakens the chemical bonds, reduces the Debye temperature and effectively optimizes the phonon transport in the system. Although the transport property of carrier does not optimize simultaneously in the present work, yet, this work demonstrates the importance of introduction of localized "rattling" mode for exploring novel cation-deficient thermoelectric materials.

ASSOCIATED CONTENT

Supporting Information

The Supporting Information is available free of charge on the ACS Publications website at DOI: 10.1021/acsami.9b12256.

EPMA mappings and average chemical compositions of Cu, In, and Te on polished samples $(Cu_2Te)_x(Cu_{3.52}In_{4.16}Te_8)$ ($x = 0$, 0.08). Microstructures observed using high resolution TEM. Differential scanning calorimetry (DSC) analysis and high temperature diffraction XRD patterns of the material at $x = 0.08$. The refinements of the powder X-ray diffraction (XRD) patterns and the refined crystallographic data of $(Cu_2Te)_x(Cu_{3.52}In_{4.16}Te_8)$ ($x = 0$, 0.05, 0.08 and 0.11). The DOS without shifting the Fermi level(s). The chosen numerical settings for phonon spectra calculation. The thermoelectric performance of the sample at $x = 0.08$ in the cooling process PDF)

AUTHOR INFORMATION

Corresponding Authors

*(Z.H.) E-mail: hegongdahuagong@126.com.
*(D.S.) E-mail: sarker@fhi-berlin.mpg.de.
*(J.C.) Phone: 86-574-87616023. Fax: 86-574-87616023. E-mail:cuijiaolin@163.com, cuijl@nbut.edu.cn.

ORCID

Jiaolin Cui: 0000-0002-4110-8347

Notes

The authors declare no competing financial interest.

ACKNOWLEDGMENTS

This work was supported by the National Natural Science Foundation of China (51671109, 51171084).

REFERENCES

(1) Biswas, K.; He, J.; I. Blum, D.; Wu, C.; Hogan, T. P.; Seidman, D. N.; Dravid, V. P.; Kanatzidis, M. G. High-performance bulk thermoelectrics with all-scale hierarchical architectures. *Nature* **2012**, *489*, 414–418.

(2) Biswas, K.; He, J.; Zhang, Q.; Wang, G.; Uher, C.; Dravid, V. P.; Kanatzidis, M. G. Strained endotaxial nanostructures with high thermoelectric figure of merit. *Nat. Chem.* **2011**, *3*, 160–166.

DOI: 10.1021/acsami.9b12256
ACS Appl. Mater. Interfaces 2019, 11, 32192–32199

(3) Zhao, W.; Liu, Z.; Sun, Z.; Zhang, Q.; Wei, P.; Mu, X.; Zhou, H.; Li, C.; Ma, S.; He, D.; Ji, P.; Zhu, W.; Nie, X.; Su, X.; Tang, X.; Shen, B.; Dong, X.; Yang, J.; Liu, Y.; Shi, J. Superparamagnetic enhancement of thermoelectric performance. *Nature* **2017**, *549*, 247−251.
(4) Liu, H.; Shi, X.; Xu, F.; Zhang, L.; Zhang, W.; Chen, L.; Li, Q.; Uher, C.; Day, T.; Snyder, G. J. Copper ion liquid-like thermoelectrics. *Nat. Mater.* **2012**, *11*, 422−425.
(5) Liu, H.; Yuan, X.; Lu, P.; Shi, X.; Xu, F.; He, Y.; Tang, Y.; Bai, S.; Zhang, W.; Chen, L.; Lin, Y.; Shi, L.; Lin, H.; Gao, X.; Zhang, X.; Chi, H.; Uher, C. Ultrahigh thermoelectric performance by electron and phonon critical scattering in $Cu_2Se_{1-x}I_x$. *Adv. Mater.* **2013**, *25*, 6607−6612.
(6) Roychowdhury, S.; Ghosh, T.; Arora, R.; Waghmare, U. V.; Biswas, K. Stabilizing n-Type cubic GeSe by entropy-driven alloying of $AgBiSe_2$: ultralow thermal conductivity and promising thermoelectric performance. *Angew. Chem., Int. Ed.* **2018**, *57*, 15167−15171.
(7) Guin, S. N.; Chatterjee, A.; Negi, D. S.; Datta, R.; Biswas, K. High thermoelectric performance in tellurium free p-type $AgSbSe_2$. *Energy Environ. Sci.* **2013**, *6*, 2603−2608.
(8) Zhang, Y.; Vidvuds, O.; Morelli, D.; Wolverton, C. Prediction of new stable compounds and promising thermoelectrics in the Cu-Sb-Se System. *Chem. Mater.* **2014**, *26*, 3427−3435.
(9) Zhang, Y.; Skoug, E.; Cain, J.; Vidvuds, O.; Morelli, D.; Wolverton, C. First-principles description of anomalously low lattice thermal conductivity in thermoelectric Cu-Sb-Se ternary semiconductors. *Phys. Rev. B* **2012**, *85*, 054306.
(10) Zhao, L.; Lo, S.; Zhang, Y.; Sun, H.; Tan, G.; Uher, C.; Wolverton, C.; Dravid, V. P.; Kanatzidis, M. G. Ultralow thermal conductivity and high thermoelectric figure of merit in SnSe crystals. *Nature* **2014**, *508*, 373−377.
(11) Jana, M. K.; Pal, K.; Waghmare, U. V.; Biswas, K. The origin of ultralow thermal conductivity in InTe: lone-pair-induced anharmonic rattling. *Angew. Chem., Int. Ed.* **2016**, *55*, 7792−7796.
(12) Samanta, M.; Pal, K.; Pal, P.; Waghmare, U.; Biswas, K. Localized vibrations of Bi bilayer leading to ultralow lattice thermal conductivity and high thermoelectric performance in weak topological insulator n-type BiSe. *J. Am. Chem. Soc.* **2018**, *140*, 5866−5872.
(13) Ying, P.; Li, X.; Wang, Y.; Yang, J.; Fu, C.; Zhang, W.; Zhao, X.; Zhu, T. Hierarchical chemical bonds contributing to the intrinsically low thermal conductivity in alpha-MgAgSb thermoelectric materials. *Adv. Funct. Mater.* **2017**, *27*, 1604145.
(14) Wang, S.; Yang, J.; Wu, L.; Wei, P.; Yang, J.; Zhang, W.; Grin, Y. Anisotropic Multicenter bonding and high thermoelectric performance in electron-poor CdSb. *Chem. Mater.* **2015**, *27*, 1071−1081.
(15) Tan, G.; Hao, S.; Zhao, J.; Wolverton, C.; Kanatzidis, M. High thermoelectric performance in electron-doped $AgBi_3S_5$ with ultralow thermal conductivity. *J. Am. Chem. Soc.* **2017**, *139*, 6467−6473.
(16) Li, W.; Lin, S.; Ge, B.; Yang, J.; Zhang, W.; Pei, Y. Low sound velocity contributing to the high thermoelectric performance of Ag_8SnSe_6. *Adv. Sci.* **2016**, *3*, 1600196.
(17) Lin, S.; Li, W.; Li, S.; Zhang, X.; Chen, Z.; Xu, Y.; Chen, Y.; Pei, Y. High thermoelectric performance of Ag_9GaSe_6 enabled by low cutoff frequency of acoustic phonons. *Joule* **2017**, *1*, 816−830.
(18) Qiu, P.; Qin, Y.; Zhang, Q.; Li, R.; Yang, J.; Song, Q.; Tang, Y.; Bai, S.; Shi, X.; Chen, L. Intrinsically high thermoelectric performance in $AgInSe_2$ n-type diamond-like compounds. *Adv. Sci.* **2018**, *5*, 1700727.
(19) Roychowdhury, S.; Jana, M.; Pan, J.; Guin, S.; Sanyal, D.; Waghmare, U.; Biswas, K. Soft phonon modes leading to ultralow thermal conductivity and high thermoelectric performance in AgCuTe. *Angew. Chem., Int. Ed.* **2018**, *57*, 4043−4047.
(20) Xu, B.; Feng, T.; Agne, M. T.; Tan, Q.; Li, Z.; Imasato, K.; Zhou, L.; Bahk, J.; Ruan, X.; Snyder, G. J.; Wu, Y. Manipulating Band Structure through Reconstruction of Binary Metal Sulfide for High-Performance Thermoelectrics in Solution-Synthesized Nanostructured $Bi_{13}S_{18}I_2$. *Angew. Chem., Int. Ed.* **2018**, *57*, 2413−2418.
(21) Chung, D.; Hogan, T.; Rocci-Lane, M.; Brazis, P.; Ireland, J.; Kannewurf, C.; Bastea, M.; Uher, C.; Kanatzidis, Mercouri. G. A new thermoelectric material: $CsBi_4Te_6$. *J. Am. Chem. Soc.* **2004**, *126*, 6414−6428.
(22) Hong, M., Wang, Y., Feng, T., Sun, Q., Xu, S., Matsumura, S., Pantelides, S., Zou, J., Chen, Z. Strong phonon−phonon interactions securing extraordinary thermoelectric $Ge_{1-x}Sb_xTe$ with Zn-alloying-induced band alignment. *J. Am. Chem. Soc.* **2019** *1411742*.
(23) Kosuga, A.; Umekage, K.; Matsuzawa, M.; Sakamoto, Y.; Yamada, I. Room-temperature pressure-induced nanostructural $CuInTe_2$ thermoelectric material with low thermal conductivity. *Inorg. Chem.* **2014**, *53*, 6844−6849.
(24) Kosuga, A.; Plirdpring, T.; Higashine, R.; Matsuzawa, M. K.; Kurosaki, M.; Yamanaka, S. High-temperature thermoelectric properties of $Cu_{1-x}InTe_2$ with a chalcopyrite structure. *Appl. Phys. Lett.* **2012**, *100*, 042108.
(25) Liu, R.; Xi, L.; Liu, H.; Shi, X.; Zhang, W.; Chen, L. Ternary compound $CuInTe_2$: a promising thermoelectric material with diamond-like structure. *Chem. Commun.* **2012**, *48*, 3818−3820.
(26) Wei, J.; Liu, H.; Cheng, L.; Zhang, J.; Liang, J. H.; Jiang, P. H.; Fan, D.-D.; Shi, J. Tuning the carrier concentration to improve the thermoelectric performance of $CuInTe_2$ compound. *AIP Adv.* **2015**, *5*, 107230.
(27) Xia, Z.; Wang, G.; Zhou, X.; Wen, W. Substitution defect enhancing thermoelectric properties in $CuInTe_2$. *Mater. Res. Bull.* **2018**, *101*, 184−189.
(28) Liu, R.; Qin, Y.; Cheng, N.; Zhang, J.; Shi, X.; Grin, Y.; Chen, L. Thermoelectric performance of $Cu_{1-x-\delta}$ Ag_xInTe_2 diamond-like materials with a pseudocubic crystal structure. *Inorg. Chem. Front.* **2016**, *3*, 1167−1177.
(29) Luo, Y.; Yang, J.; Jiang, Q.; Li, W.; Zhang, D.; Zhou, Z.; Cheng, Y.; Ren, Y.; He, X. Progressive regulation of electrical and thermal transport properties to high-performance $CuInTe_2$ thermoelectric materials. *Adv. Energy Mater.* **2016**, *6*, 1600007.
(30) Luo, Y.; Jiang, Q.; Yang, J.; Li, W.; Zhang, D.; Zhou, Z.; Cheng, Y.; Ren, Y.; He, X.; Li, X. Simultaneous regulation of electrical and thermal transport properties in $CuInTe_2$ by directly incorporating excess ZnX (X = S,Se). *Nano Energy* **2017**, *32*, 80−87.
(31) Xia, Z.; Wang, G.; Zhou, X.; Wen, W. Effect of the Cu vacancy on the thermoelectric performance of p-type $Cu_{1-x}InTe_2$ compounds. *Ceram. Int.* **2017**, *43*, 16276−16282.
(32) Cheng, N.; Liu, R.; Bai, S.; Shi, X.; Chen, L. Enhanced thermoelectric performance in Cd doped $CuInTe_2$ compounds. *J. Appl. Phys.* **2014**, *115*, 163705.
(33) Shen, J.; Zhang, X.; Lin, S.; Li, J.; Chen, Z.; Li, W.; Pei, Y. Vacancy scattering for enhancing the thermoelectric performance of $CuGaTe_2$ solid solutions. *J. Mater. Chem. A* **2016**, *4*, 15464−15470.
(34) Zhang, J.; Liu, R.; Cheng, N.; Zhang, Y.; Yang, J.; Uher, C.; Shi, X.; Chen, L.; Zhang, W. High-performance pseudocubic thermoelectric materials from non-cubic chalcopyrite compounds. *Adv. Mater.* **2014**, *26*, 3848−3853.
(35) Shi, X.; Chen, L.; Uher, C. Recent advances in high-performance bulk thermoelectric materials. *Int. Mater. Rev.* **2016**, *61*, 379−415.
(36) Zhu, J.; Luo, Y.; Cai, G.; Liu, X.; Du, Z.; Tang, F.; Cui, J. Significant improvement in the thermoelectric performance of Sb-incorporated chalcopyrite compounds $Cu_{18}Ga_{25}Sb_xTe_{50-x}$ (x = 0−3.125) through the coordination of energy band and crystal structures. *J. Mater. Chem. A* **2017**, *5*, 24199−24207.
(37) Li, M.; Luo, Y.; Cai, G.; Li, X.; Li, X.; Han, Z.; Lin, X.; Sarker, D.; Cui, J. Realizing high thermoelectric performance in Cu_2Te alloyed $Cu_{1.15}In_{2.29}Te_4$. *J. Mater. Chem. A* **2019**, *7*, 2360−2367.
(38) Ren, T.; Ying, P.; Cai, G.; Li, X.; Han, Z.; Min, L.; Cui, J. Improvement of thermoelectric performance of copper-deficient compounds $Cu_{2.5+\delta}In_{4.5}Te_8$ (δ=0−0.15) due to degenerate impurity band and ultralow lattice thermal conductivity. *RSC Adv.* **2018**, *8*, 27163−27170.
(39) Kim, H.; Gibbs, Z. M.; Tang, Y.; Wang, H.; Snyder, G. J. Characterization of Lorenz number with Seebeck coefficient measurement. *APL Mater.* **2015**, *3*, 041506.

DOI: 10.1021/acsami.9b12256
ACS Appl. Mater. Interfaces 2019, 11, 32192−32199

(40) Blum, V.; Gehrke, R.; Hanke, F.; Havu, P.; Havu, V.; Ren, X.; Reuter, K.; Scheffler, M. Ab initio molecular simulations with numeric atom-centered orbitals. *Comput. Phys. Commun.* **2009**, *180*, 2175.
(41) Hohenberg, P.; Kohn, W. Inhomogeneous electron gas. *Phys. Rev.* **1964**, *136*, B864.
(42) Kohn, W.; Sham, L. J. Self-consistent equations including exchange and correlation effects. *Phys. Rev.* **1965**, *140*, A1133.
(43) Perdew, J. P.; Burke, K.; Ernzerhof, M. Generalized gradient approximation made simple. *Phys. Rev. Lett.* **1998**, *77*, 3865.
(44) Krukau, A. V.; Vydrov, O. A.; Izmaylov, A. F.; Scuseria, G. E. Influence of the exchange screening parameter on the performance of screened hybrid functionals. *J. Chem. Phys.* **2006**, *125*, 224106.
(45) Togo, A.; Oba, F.; Tanaka, I. First-principles calculations of the ferroelastic transition between rutile-type and $CaCl_2$-type SiO_2 at high pressures. *Phys. Rev. B: Condens. Matter Mater. Phys.* **2008**, *78*, 134106.
(46) Zunger, A. Order-disorder transformation in ternary tetrahedral semiconductors. *Appl. Phys. Lett.* **1987**, *50*, 164−166.
(47) Schorr, S.; Geandier, G.; Korzun, B. V. Some are different from others: high temperature structural phase transitions in ternary chalcopyrites. *Phys. Status Solidi C* **2006**, *3*, 2610−2613.
(48) Rinón, C. On the order-disorder phase transition in ternary compounds. *Solid State Commun.* **1987**, *64*, 663−665.
(49) Tan, G.; Shi, F.; Hao, S.; Chi, H.; Bailey, T. P.; Zhao, L.; Uher, C.; Wolverton, C.; Dravid, V. P.; Kanatzidis, M. G. Valence band modification and high thermoelectric performance in SnTe heavily alloyed with MnTe. *J. Am. Chem. Soc.* **2015**, *137*, 11507−11516.
(50) Liu, X.; Zhu, T.; Wang, H.; Hu, L.; Xie, H.; Jiang, G.; Snyder, G. J.; Zhao, X. Low electron scattering potentials in high performance $Mg_2Si_{0.45}Sn_{0.55}$ based thermoelectric solid solutions with band convergence. *Adv. Energy Mater.* **2013**, *3*, 1238−1244.
(51) Khan, A. U.; Orabi, R.; Pakdel, A.; Vaney, J. B.; Fontaine, B.; Gautier, R.; Halet, J. F.; Mitani, S.; Mori, T. Sb doping of metallic $CuCr_2S_4$ as a route to highly improved thermoelectric properties. *Chem. Mater.* **2017**, *29*, 2988−2996.
(52) Heinrich, C. P.; Day, T. W.; Zeier, W. G.; Snyder, G. J.; Tremel, W. Effect of isovalent substitution on the thermoelectric properties of the $Cu_2ZnGeSe_{4-x}S_x$ series of solid solutions. *J. Am. Chem. Soc.* **2014**, *136*, 442−448.
(53) Lin, H.; Tan, G.; Shen, J.; Hao, S.; Wu, L.; Calta, N.; Malliakas, C.; Wang, S.; Uher, C.; Wolverton, C.; Kanatzidis, M. G. Concerted rattling in $CsAg_5Te_3$ leading to ultralow thermal conductivity and high thermoelectric performance. *Angew. Chem., Int. Ed.* **2016**, *55*, 11431−11436.
(54) Shi, Y.-X.; Assoud, A.; Ponou, S.; Lidin, S.; Kleinke, H. A new material with a composite crystal structure causing ultralow thermal conductivity and outstanding thermoelectric properties: $Tl_2Ag_{12}Te_{7+\delta}$. *J. Am. Chem. Soc.* **2018**, *140*, 8578−8585.
(55) Lin, C.; Lydia, R.; Yun, J. H.; Lee, H. S.; Rhyee, J. S. Extremely low lattice thermal conductivity and point defect scattering of phonons in Ag-doped $(SnSe)_{1-x}(SnS)_x$ compounds. *Chem. Mater.* **2017**, *29*, 5344−5352.
(56) Zhang, X.; Chen, Z.; Lin, S.; Zhou, B.; Gao, B.; Pei, Y. Promising thermoelectric $Ag_{5-\delta}Te_3$ with intrinsic low Lattice thermal conductivity. *ACS Energy Lett.* **2017**, *2*, 2470−2477.
(57) Li, J.; Wu, H.; Wu, D.; Wang, C.; Zhang, Z.; Li, Y.; Liu, F.; Ao, W.; He, J. Extremely low thermal conductivity in thermoelectric $Ge_{0.55}Pb_{0.45}Te$ solid solutions via Se substitution. *Chem. Mater.* **2016**, *28*, 6367−6373.
(58) Cahill, D. G.; Watson, S. K.; Pohl, R. O. Lower limit to the thermal conductivity of disordered crystals. *Phys. Rev. B: Condens. Matter Mater. Phys.* **1992**, *46*, 6131.
(59) Zheng, Z.; Su, X.; Deng, R.; Stoumpos, C.; Xie, H.; Liu, W.; Yan, Y.; Hao, S.; Uher, C.; Wolverton, C.; Kanatzidis, M. G.; Tang, X. Rhombohedral to cubic conversion of GeTe via MnTe alloying leads to ultralow thermal conductivity, electronic band convergence, and high thermoelectric performance. *J. Am. Chem. Soc.* **2018**, *140*, 2673−2686.
(60) Chen, Z.; Zhang, X.; Lin, S.; Chen, L.; Pei, Y. Rationalizing phonon dispersion for lattice thermal conductivity of solids. *Natl. Sci. Rev.* **2018** 5888.
(61) Zhou, C.; Yu, Y.; Lee, Y.; Cojocaru-Mirédin, O.; Yoo, B.; Cho, Sung-Pyo.; Im, J.; Wuttig, M.; Hyeon, T.; Chung, I. High-performance n-type PbSe−Cu_2Se thermoelectrics through conduction band engineering and phonon softening. *J. Am. Chem. Soc.* **2018**, *140*, 15535−15545.
(62) Xiao, Y.; Wu, H.; Li, W.; Yin, M.; Pei, Y.; Zhang, Y.; Fu, L.; Chen, Y.; Pennycook, S. J.; Huang, L.; He, J.; Zhao, L. Remarkable roles of Cu to synergistically optimize phonon and carrier transport in n-type PbTe-Cu_2Te. *J. Am. Chem. Soc.* **2017**, *139*, 18732−18738.
(63) Fernandez, B.; Wasim, S. M. Sound velocities and elastic moduli in $CuInTe_2$, and $CuInSe_2$. *Phys. stat. sol. (a)* **1990**, *122*, 235−242.
(64) Plirdpring, T.; Kurosaki, K.; Kosuga, A.; Day, T.; Firdosy, S.; Ravi, V.; Snyder, G. J.; Adul Harnwunggmoung, A.; Sugahara, T.; Ohishi, Y.; Muta, H.; Yamanaka, S. Chalcopyrite $CuGaTe_2$: A high-efficiency bulk thermoelectric material. *Adv. Mater.* **2012**, *24*, 3622−3626.
(65) Zhang, L.; Zheng, Q.; Xie, Y.; Lan, Z.; Prezhdo, O. V.; Saidi, W. A.; Zhao, J. Delocalized impurity phonon induced electron-hole recombination in doped semiconductors. *Nano Lett.* **2018**, *18*, 1592.
(66) Zhao, X.; Wu, Z.; Cui, W.; Zhi, Y.; Guo, D.; Li, L.; Tang, W. Impurity compensation effect induced by tin valence change in α-$Ga_{1.4}Sn_{0.6}O_3$ thin films. *ACS Appl. Mater. Interfaces* **2017**, *9*, 983−988.
(67) Butt, S.; Xu, W.; Farooq, M. U.; Ren, G. K.; Zhang, Q.; Zhu, Y. C.; Khan, S. U.; Liu, L.; Yu, M.; Mohmed, F.; Lin, Y.; Nan, C. Enhanced thermoelectricity in high-temperature β-Phase copper(I) selenides embedded with Cu_2Te nanoclusters. *ACS Appl. Mater. Interfaces* **2016**, *8*, 15196−15204.
(68) Cui, J.; Zhu, J.; Han, Z.; Luo, Y. Significantly improved thermal stability and thermoelectric performance of u-deficient $Cu_{4-\delta}Ga_4Te_8$ (δ=1.12) chalcogenides through addition of Sb. *J. Mater. Chem. A* **2018**, *6*, 12672−12681.
(69) Hu, L.; Zhu, T.; Liu, X. H.; Zhao, X. Point defect engineering of high-performance bismuth-telluride-based thermoelectric materials. *Adv. Funct. Mater.* **2014**, *24*, 5211−5218.
(70) Caillat, T.; J. Fleurial, J.; Borshchevsky, A. Preparation and thermoelectric properties of semiconducting Zn_4Sb_3. *J. Phys. Chem. Solids.* **1997**, *58*, 1119−1125.
(71) Snyder, G.; Toberer, E. S. Complex thermoelectric materials. *Nat. Mater.* **2008**, *7*, 105−114.

DOI: 10.1021/acsami.9b12256
ACS Appl. Mater. Interfaces 2019, 11, 32192−32199